Crystal structure of bent carbon dioxide phase IV

J.-H. Park,[1] C. S. Yoo,[1,4] V. Iota,[1] H. Cynn,[1] M. F. Nicol,[2,4] and T. Le Bihan[3]
[1]*High Pressure Physics Group, Physics and Advanced Technologies, Lawrence Livermore National Laboratory, Livermore, California 94551, USA*
[2]*High Pressure Science and Engineering Center, University of Nevada, Las Vegas, Nevada 89154-4002, USA*
[3]*European Synchrotron Radiation Facility, BP 220, F-38043 Grenoble Cedex, France*
[4]*High Pressure Collaborative Access Team, Advanced Photon Source, Argonne National Laboratory, Argonne, Illinois 60439, USA*
(Received 9 December 2002; published 18 July 2003)

The crystal structure of carbon dioxide phase IV (CO_2-IV) has been characterized based on powder angle-resolved x-ray diffraction data obtained *in situ* at 300–750 K and 11–50 GPa. The results confirm that in this high-pressure polymorph O═C═O molecules are nonlinear. Rietveld analyses of the x-ray data yield two plausible structures: $P4_12_12$ (α-SiO_2 cristobalite) and *Pbcn* (α-PbO_2, post-stishovite). Carbon dioxide molecules are bent slightly more in the *Pbcn* phase ($<$C-O-C$=160°$) than in the $P4_12_12$ (171°). For both structures, the intramolecular C-O bond is increased to 1.50($\pm$0.1) Å at the distance of a C-O single bond, whereas the intermolecular C$\cdots$O distance is reduced to around 2.1($\pm$0.2) Å. The bending and elongation of the molecular units suggest that phase IV is an intermediate state between the molecular and nonmolecular extended phases and that the molecular-to-nonmolecular transformation in carbon dioxide occurs gradually via intermediate phases IV and II. Transition pathways among all five CO_2 phases (I–V) are also discussed in the context of symmetry arguments and transition mechanisms. Considerations of plausible mechanisms of the transitions among phases I, II, IV, and V favor the *Pbcn* interpretation of the crystal structure of phase IV.

DOI: 10.1103/PhysRevB.68.014107 PACS number(s): 64.70.Kb, 62.50.+p, 71.15.Nc

INTRODUCTION

Pressure-induced electron delocalization has well been recognized for many years as observed in the insulator-to-metal transitions of Xe[1,2] and H_2[3,4]) and more recently in the molecular-to-nonmolecular phase transitions of CO_2[5,6] and N_2.[7,8] These pressure-induced changes in such simple systems provide an excellent test bed to develop new condensed matter theory[9–11] as well as a great opportunity to discover novel phases and exotic materials. As a result, it is quite clear that high pressure is rapidly establishing its important role in materials research. Despite such importance, high-pressure materials research, however, has remained largely exploratory, partly owing to the formidable high-pressure and temperature conditions that often hinder one from obtaining fundamental materials data such as the crystal structure, transition mechanism, and lattice dynamics.

Carbon dioxide is a good example of a material with a richness of high-pressure polymorphs and a great diversity in intermolecular interactions, chemical bonding, and crystal structures.[12] Solid CO_2 ranges from a typical molecular phase I ($Pa\bar{3}$)[13] observed below 10 GPa and 700 K to a fully extended, polymeric phase V ($P2_12_12_1$)[6] above 40 GPa and 1800 K. Between these extreme of pressure and temperature, three additional phases have been discovered. The cubic phase I ($Pa\bar{3}$) transforms to the orthorhombic phase III (*Cmca*)[14] above 11 GPa at temperatures below 450 K. Upon subsequent heating at 20 GPa, phase III transforms to a pseudotetragonal phase II ($P4_2/mnm$ or *Pnnm*)[15] above $\sim$500 K and then to phase IV above $\sim$1000 K.

The pathways and dynamics of the transitions among CO_2 phases are rather complicated because of the strong kinetic barriers associated with some of these transitions. Phase IV, for example, can also be produced without remnants of phase II by directly laser-heating phase III at pressures between 10 and 30 GPa.[16] Both phases II and IV are recoverable at ambient temperature at pressures well within the stability field of the phase III. Laser heating of quenched CO_2-IV further transforms it to the extended phase V above 30 GPa, which is substantially lower than the pressure where phase III transforms to V upon laser heating. In this respect, phase IV behaves as a precursor for forming CO_4 tetrahedra like those making up phase V. Such multiple pathways to the phase V from both phases III and IV make it difficult to determine the exact thermodynamic phase boundaries above 30 GPa and 1000 K. In fact, a recent study suggests that yet another phase VI[17] occurs in the pressure-temperature region overlapping with phases IV and V.

The existence of the phases II, III, and IV at intermediate pressure-temperature conditions suggests that the molecular-to-nonmolecular transformation may occur via intermediates different from either the quadrupole-quadrupole interacting molecules of phase I or the covalently bonded extended phase V. For example, phase III[6] supports extremely high strains, evident from its characteristic textures and its ability to support a large pressure gradient near 100–200 GPa/mm, both of which are quite unusual for a molecular solid. The crystal structure of phase II[15] shows an elongated intramolecular C═O bond to around 1.33 Å bond, collapsed intermolecular C$\cdots$O bond near 2.33 Å, and nearest O$\cdots$O contacts intermediate between those of molecular and extended phases. The Raman spectrum of phase IV[16] clearly includes ν_2 bending modes, indicating that CO_2 molecules are bent and, thus, the intermolecular interactions are much stronger in this phase.

Because the stability field of phase IV occurs between

those of molecular phase I and extended phase V,[12] detailed structural information about phase IV is critical for achieving a better understanding of the transition pathways, transition dynamics, and stabilities (or metastabilities) of the phases governing the molecular-to-nonmolecular phase transition. In this paper we report the crystal structure of phase IV obtained from the angle-resolved synchrotron x-ray diffraction experiments *in situ* between 300 and 750 K above 11 GPa and, based on crystal symmetry arguments, offer some plausible explanations for the transition pathways among all five (I–V) phases of CO_2.

EXPERIMENTS

Carbon dioxide samples were loaded into diamond-anvil cells by condensing gaseous CO_2 (99.99% pure) contained in a pressure vessel at -40 °C and 10 atm. The initial compression during loading typically produced phase I, and further compression transformed phase I to phase III above 11 GPa at ambient temperature. Phase IV was then synthesized by externally heating phase III to temperatures between 500 and 750 K at pressures between 11 and 20 GPa, respectively.

Heating was achieved by an external heater (Omega) wrapped around the diamond-anvil cell which could heat the sample to 750 K at pressures up to 50 GPa. The sample temperature was measured with a precision of ~1 K by using a calibrated thermocouple (K type) in contact with the anvils. A small amount of a H_2/Ar mixture (1% H_2) was continuously flowed to avoid oxidizing diamond above 600 K. A few micron-sized ruby ($Al_2O_3:Cr^{3+}$) crystals were loaded in the cell, and the pressure was determined based on the previously reported temperature-adjusted ruby luminescence.[18] Because each CO_2 phase has a distinctive visual appearance, a characteristic Raman spectrum, and a characteristic x-ray diffraction pattern, one can unambiguously probe the phase transitions from CO_2-III to CO_2-II and subsequently to CO_2-IV, with increasing temperature. The reproducibility of these properties over broad ranges of pressure and temperature implies that, once formed, phase IV can be quenched at ambient temperature between 11 and 20 GPa as a single phase without remnants of any other phases.

Above 20 GPa, because of the relatively high temperature required to make phase IV, it was typically made by laser-heating CO_2-III. Despite a large temperature gradient within the laser-heated area, the laser-quenched sample was typically a mixture of phase IV and unconverted phase III, without any apparent phase II. This result implies that phase transitions among III, II, and IV involve large kinetic barriers and that phase IV probably forms directly from phase III during laser heating. No differences were apparent between phase-IV samples quenched from laser-heating experiments and external-heating experiments. However, when pressure on quenched phase-IV material is further increased at ambient temperature, broadening of the Raman spectra shows that strong lattice distortions develop; indeed, these distortions may mean that quenched phase IV transforms into yet another new phase upon compression at ambient temperature above ~30 GPa.[16] Because of these complications, lattice distortions, and the possible phase transition of the quenched phase IV upon further compression, we only discuss in this paper the crystal structures of "*in situ*" and "as-quenched" samples of the phase IV from external heating experiments. The details of pressure-induced Raman changes and phase transitions of phase IV have previously been reported elsewhere.[16]

Angle-resolved powder x-ray diffraction (ADXD) data of CO_2-IV samples were collected by using focused monochromatic synchrotron x-rays at $\lambda = 0.3738$ Å from double undulators at the ID-30 of the European Synchrotron Radiation Facility (ESRF) and at $\lambda = 0.6199$ Å from a wiggler at the BL 10-2 of the Stanford Synchrotron Radiation Laboratory (SSRL). A series of Debye-Sherrer diffraction rings was recorded between $2\theta = 5°$ and 35° on high-resolution image plates (MAR 345 at the ESRF and Fuji BAS2500 at the SSRL). The FIT2D program[19] was then employed to convert the two-dimensional (2D) image-plate records into 1D data for structural refinement by using the GSAS routines.[20]

RESULTS

Figure 1 shows a typical ADXD pattern of CO_2-IV at 15 GPa and ambient temperature, together with the calculated and difference diffraction patterns. The diffraction pattern can be indexed to either a tetragonal unit cell with $a_T = 4.335(7)$ Å and $c_T = 6.102(3)$ Å or a pseudotetragonal unit cell with $a_O = 4.3441(8)$ Å, $b_O = 6.111(3)$ Å, and $c_O = 4.285(1)$ Å, with the exceptions on several weak features originated from rhenium gasket and diamond scattering. Note that these two cells are very similar to each other, $a_T \sim a_O \sim c_O$ and $c_T = b_O$, as well as are very close to a cubic cell, $\sqrt{2} \cdot a_T$ (a_O or c_O) $= c_T$ (or b_O) $= a_C \approx 6.10$ (± 0.05) Å. However, the peak splitting at higher angles (20°–24°) and the intensity data indicate that the symmetry is lower than cubic and favors the tetragonal or pseudotetragonal structure.

The observed extinction conditions of the tetragonal cell are k = even for $(0k0)$ and $l = 4n$ for $(00l)$, which correspond to the space group $P4_12_12$. The refined intensity is in a good agreement with the observed one with the R factors of $R_{wp} = 2.71\%$, $R_p = 2.35\%$, reduced $\chi^2 = 1.286$, and $R(F^2) = 0.2424$, the texture index of 2.1, and zero shift of -0.11 (Ref. 21). The final refined positions of C ($4a$) and O ($8b$) are, respectively, (0.460(2), 0.460(2), 0) and (0.262(2), 0.218(2),0.260(1)), while the corresponding displacement parameters are 0.146(10) and 0.087(3) Å^2.

Considering peak overlaps and broadness, the diffraction pattern also appears to match with the systematic absences of orthorhombic *Pbcn*. Again, this is nearly a tetragonal cell with a small difference, ~1.5%, in the a and c unit cell parameters. The refined results are as good as the $P4_12_12$, with the R factors of $R_{wp} = 2.70\%$, $R_p = 2.31\%$, reduced $\chi^2 = 1.076$, and $R(F^2) = 0.222$ with 2.9 of the texture index and zero shift -5.1. The final refined atomic positions are C ($4c$) (0,0.323(4),0.25) and O ($8d$) (0.272(2),0.370(2),0.467(2)). The displacement parameters are 0.169(9) Å^2 for carbon and 0.084(4) Å^2 for oxygen.

Both structures generate patterns relatively well matched to the observations and, based on the R factors and χ values,

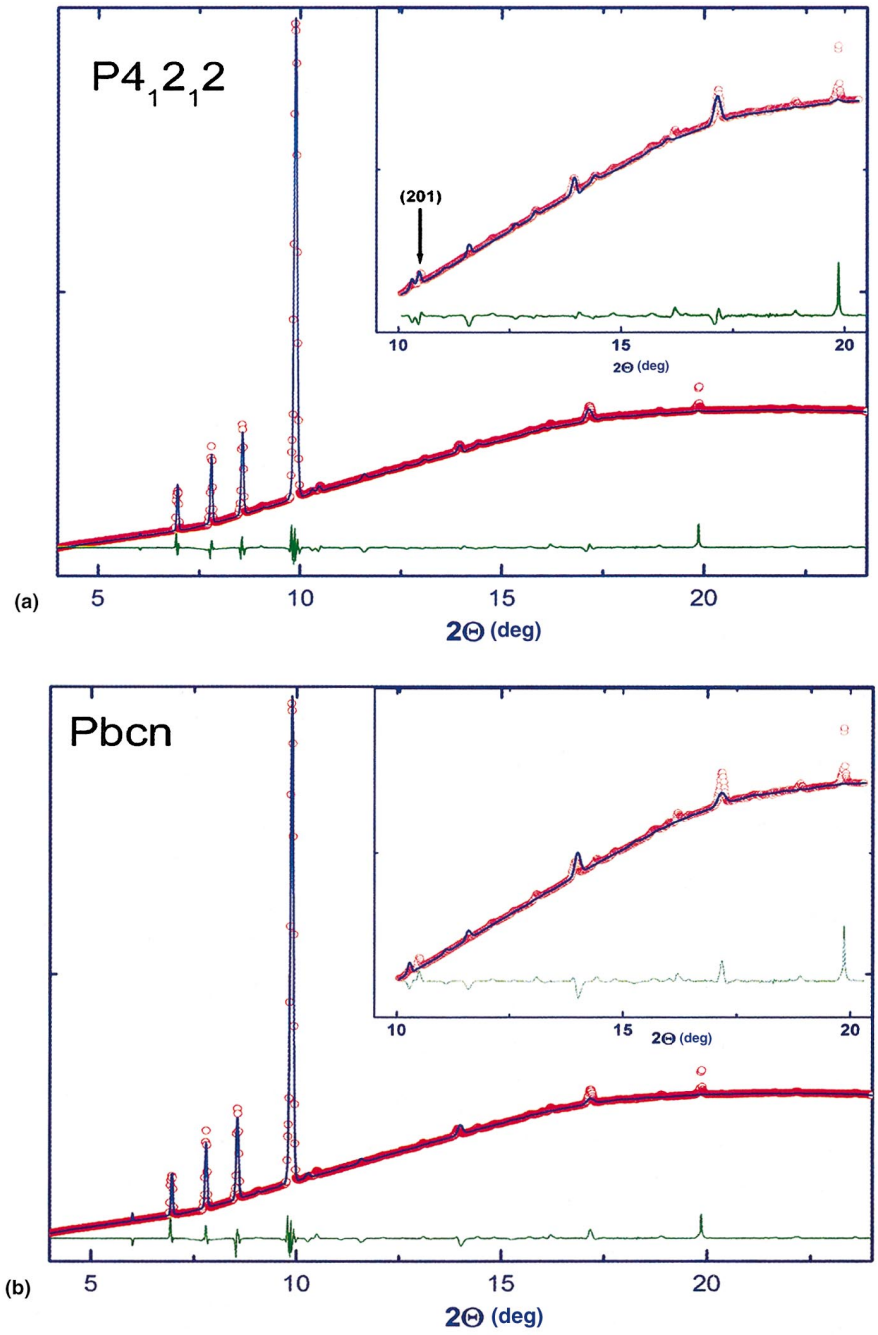

FIG. 1. (Color) Rietveld refinements of the X-ray diffraction pattern of Phase IV based on two space groups, $P4_12_12$ (a) and *Pbcn* (b), at 15 GPa and ambient temperature. The difference spectrum is also shown in a same scale.

it is difficult to distinguish one being better than the other. Therefore, in this paper we shall first present the crystal structures of both models and then discuss aspects of the transition dynamics which suggest that phase IV has the *Pbcn* structure.

Figure 2 illustrates the crystal structure of CO_2-IV based on (a) $P4_12_12$ and (b) *Pbcn*. The $P4_12_12$ structure is isostructural to low-temperature β-cristobalite.[22] It has four molecules per unit cell: two molecules along the [110] and two molecules along [110] in alternating *ab* planes. This structure can be considered as a twin cell of phase II ($P4_2/mnm$) along the *c* axis, resulting from a slight bending of CO_2 molecules. Similarly to the situation in phase II,[15] carbon atoms in phase IV can be considered as pseudo six folded with oxygen atoms at the apices of highly distorted octahedra; those oxygen atoms are two oxygen atoms bonded at 1.487(8) Å and two pairs of nonbonded oxygen atoms at 2.093(9) and 2.362(9) Å. We attribute the small disparity in nonbonded C···O distances to the small bending in the O-C-O angle at 171.4(0)°. Because of this molecular bending, nearest nonbonded O···O distance is slightly farther apart, 2.506(9) Å, than that in phase II (2.303 Å), relieving an instability of shear-type vibrations in the *ab* plane.[17]

The *Pbcn* structure is, on the other hand, isostructural to a post-stishovite α-PbO_2 structure,[23] previously found in TiO_2[24] and SnO_2[25–28] at high pressures. In this structure, the carbon atoms are neighbored by two bonded oxygen atoms at 1.5334(4) Å and two pairs of nonbonded ones at 1.964(4)

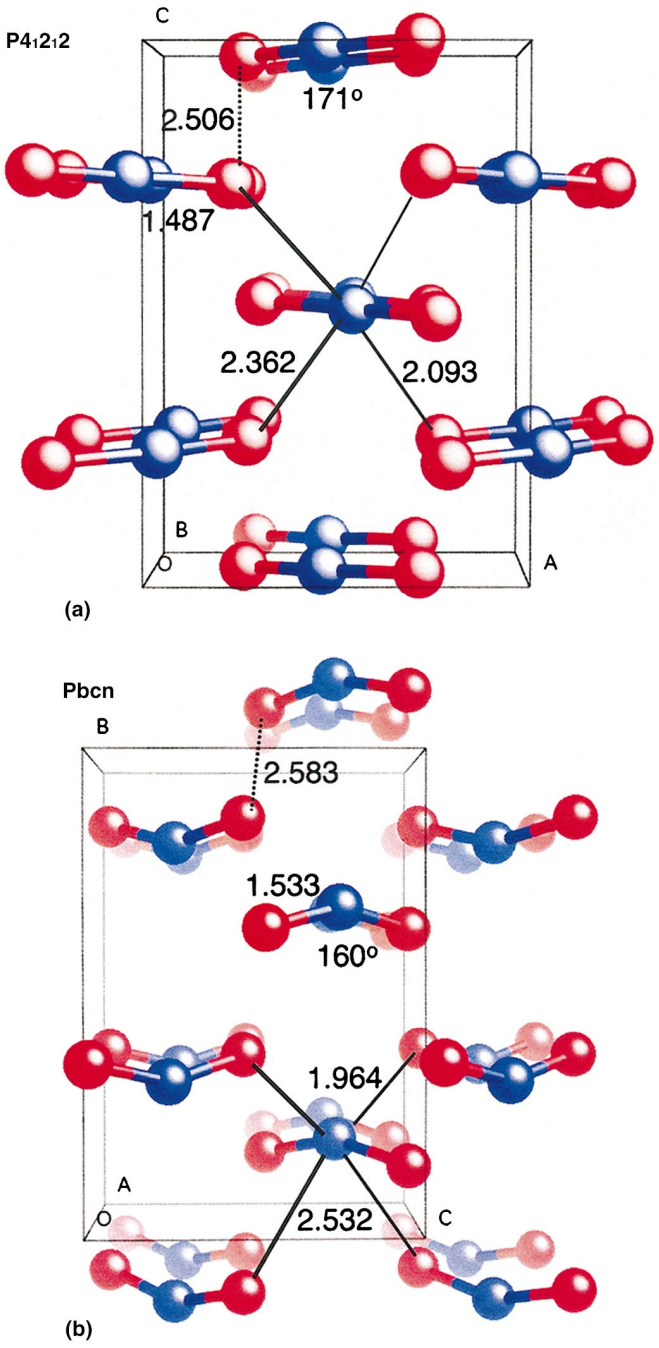

FIG. 2. (Color) The crystal structure of CO_2-IV refined in the space groups of (a) $P4_12_12$ and (b) *Pbcn*. Each unit cell contains four bent CO_2 molecules, as suggested in the previous Raman studies.[16]

and 2.532(4) Å. The larger disparity in the nonbonded C···O distance is apparently due to the larger bending in the O-C-O angle at 160.0(1)°. By the closest intermolecular C···O bonds, CO_2 molecules form buckled C-O layers parallel to the *ac* plane. In each layer, four carbon atoms and four oxygen atoms form an eight-membered ring with two C-O alternating bonds 1.533(4) and 1.964(4) Å by the angle of 97.1(1)°.

In both structures, the intramolecular C-O bond is highly

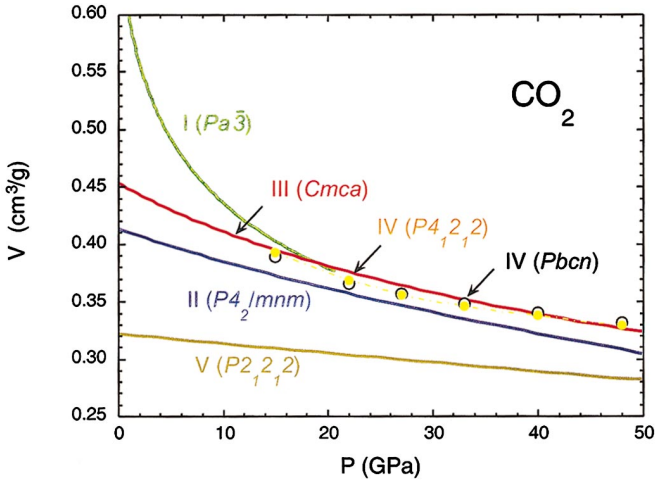

FIG. 3. (Color) Pressure-volume relationships of CO_2-IV in the two proposed structures, *Pbcn* (open circles) and $P4_12_12$ (solid circles), in comparison with those of other CO_2 phases. Note that the specific volume of CO_2-IV is between CO_2-II and III.

elongated to be in the range of C-O single bonds [~1.50 (±0.1) Å][6] as opposed to C═O double bonds (~1.20 Å).[14] The intermolecular distance, on the other hand, is substantially shorter than twice the C-O intramolecular bond distance. Based on the long intramolecular bond length and short intermolecular distance, phase IV should be considered as an intermediate state between a molecular crystal and an extended solid. The nature of phase IV is therefore analogous to that of phase II, but is even closer to extended phase V.

Pressure-volume curves of the two proposed structures are illustrated and compared with those of other phases in Fig. 3. All lattice parameters at several pressures and temperatures are also summarized in Table I. Both structures yield very similar specific volumes within 1%. The volume of phase IV is between those of phases III and II. That phase IV is denser than phase III clearly results from the higher coordination number (between 4 and 6) of carbon atoms and the shorter intermolecular C···O distances in phase IV. The higher density of phase IV and its position relative to other phases in *P-T* space also suggest that it is thermodynamically more stable than phase III. On the other hand, the carbon atoms in phase IV are more fourfoldlike than sixfold, as distinct from the pseudosixfold carbon atoms in phase II. As a result, the specific volume of phase IV is larger than that of phase II, which is consistent with the slope of the II-IV boundary.

Raman spectra of quenched phase IV between 10 and 30 GPa exhibit at least eight well-resolved lattice phonons in the region between 100 and 500 cm^{-1}, as shown in Fig. 4. These Raman data clearly suggest that the symmetry of crystal structure of phase IV is substantially lower than the *c*-centered structure of phase III, which is consistent with the two proposed primitive unit cells with four molecules. For example, factor group analyses of these crystal structures yield 12 Raman-active lattice modes ($\Gamma_{\text{Raman}}=2A_g+4B_{1g}+2B_{2g}+4B_{3g}$) for the *Pbcn*, all of which may be nondegenerate, and 18 Raman-active modes ($\Gamma_{\text{Raman}}=2A_1+4B_1+2B_2+5E$) for the $P4_12_12$, but only 13 nondegenerate

TABLE I. Lattice parameters of phase IV as refined in *Pbcn* and $P4_12_12$ space groups, at several high pressures and temperatures.

		Pbcn				$P4_12_12$		
P (GPa)	T (°C)	a_0 (Å)	b_0 (Å)	c_0 (Å)	V_O (Å^3)	a_t (Å)	c_t (Å)	V_t (Å^3)
15	25	4.344	6.111	4.285	113.75	4.336	6.102	114.71
22	25	4.199	5.984	4.252	106.83	4.255	5.943	107.61
27	25	4.130	5.759	4.390	104.41	4.224	5.829	104.02
33	25	4.111	5.895	4.203	101.87	4.221	5.683	101.25
40	25	4.076	5.848	4.176	99.54	4.141	5.764	98.85
48	25	4.004	5.793	4.181	96.96	4.137	5.631	96.37
15	25	4.344	6.111	4.285	113.75	4.336	6.102	114.72
15	49	4.365	6.134	4.335	116.07	4.334	6.104	114.65
16	156	4.344	6.139	4.337	115.66	4.344	6.120	115.49
18	200	4.330	6.124	4.331	117.02	4.335	6.113	114.88
18	275	4.354	6.148	4.350	116.44	4.342	6.130	115.57

bands. Therefore, the Raman spectrum of the quenched CO_2-IV is not determinative, considering the possible degeneracy of the observed bands.

DISCUSSION

Recall that the lattice parameters of the two proposed structures closely resemble those of a cubic structure. Such pseudocubic distortions are not rare. For example, high-temperature α-cristobalite SiO_2 (cubic, $Fd\bar{3}m$) also adopts a similar distortion to β-cristobalite (tetragonal, $P\bar{4}2_12$) upon cooling below 500 K.[29] Furthermore, the $Pa\bar{3}$ structure of CO_2-I is similar to the $Fd\bar{3}m$ of α-SiO_2 in that all carbon and silicon atoms are at fcc sites. The only difference is that oxygen atoms in α-SiO_2 are centered between nearest silicon atoms (1/4,1/4,1/4), whereas in CO_2-I they are asymmetrically driven closer to one than the other.[14] In this respect, the high-temperature distortion from CO_2-I (cubic $Pa\bar{3}$) to CO_2-IV (either tetragonal $P4_12_12$ or pseudotetragonal *Pbcn*) seems to resemble the pseudocubic distortion occurring in the α-to-β phase transition in SiO_2. Furthermore, temperature effect on the pseudocubic distortion is clearly shown by plotting the change in a_0/b_0 and c_0/b_0 in Fig. 5. The cell parameters obtained at room tem-

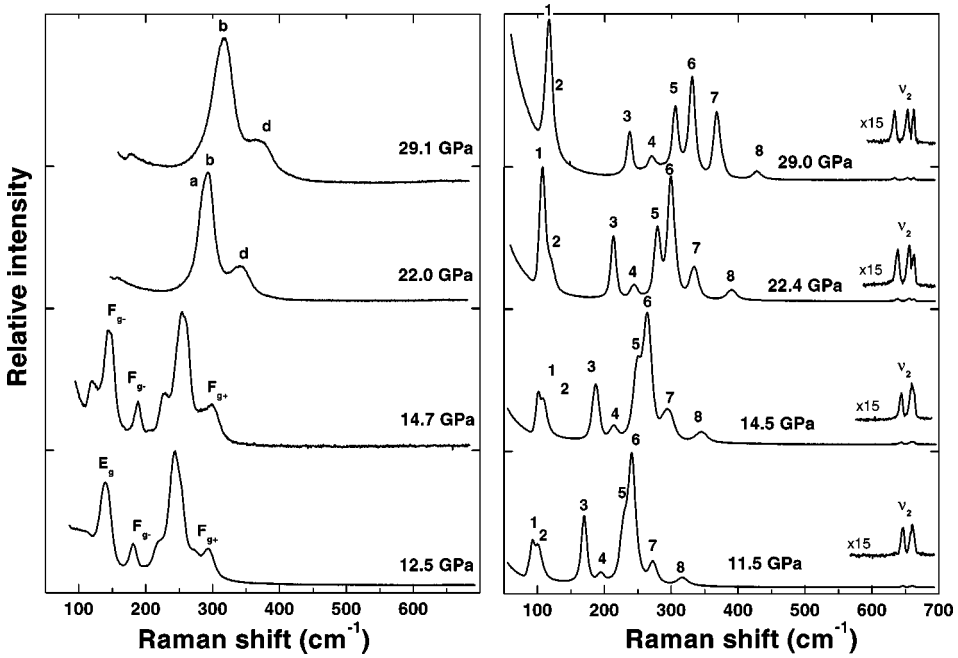

FIG. 4. Raman spectra of CO_2-IV (right) as quenched after laser heating CO_2-III (left) at several high pressures. Note that CO_2 exists as a mixture of phase I and III between 10 and 20 GPa. Phase IV is quenchable without any back transformation to phase III or II in the entire pressure range between 10 and 30 GPa. The presence of ν_2 bending modes near 650 cm^{-1} in phase IV is consistent with the bent structure of CO_2 molecules found in the present x-ray study.

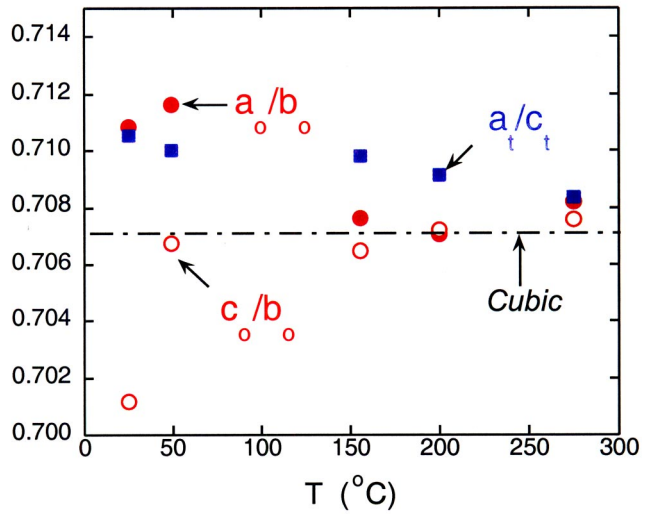

FIG. 5. The pseudo-cubic character of CO_2-IV as a function of temperature at 15 GPa. The pseudo-cubic distortion nearly diminishes within 0.8% above 150 C.

perature deviate within 0.8%. As the temperature increases, the distortion nearly diminishes to a cubic condition of $a_0/b_0=c_0/b_0=1/\sqrt{2}$ ($\sim$0.7071).

The transitions among the various carbon dioxide phases can be understood as shown in Fig. 6. For example, consider the phase transition from phase II to phase IV (*Pbcn*). Both the rutile (or $CaCl_2$) structure of phase II and the α-PbO_2 structure of phase IV are based on hcp oxygen sublattices forming highly distorted octahedral as shown in Fig. 6(a). Therefore, the oxygen positions in phases II and IV are similar. Carbon atoms, on the other hand, fill a half of those octahedral sites in phase IV, while they form straight chains through edge-sharing octahedral in phase II.[15] As a result, the II-IV phase transition involves reconstruction of mostly carbon atoms; that is, the shift of every other carbon atoms by $\frac{1}{2}$ (0,1,0) as indicated by arrows in Fig. 6(a). This motion produces the layers of zigzag chains—the α-PbO_2 structure. Such a reconstructive transformation certainly requires a large activation energy and, thus, is consistent with the previously reported sluggishness of the II-IV phase transition.[12]

The phase transformation from I ($Pa3$) to IV (*Pbcn*) also changes both the carbon and oxygen sublattices. Recall that the *a* and *c* axes of phase IV are nearly same with $c/\sqrt{2}$, which is also similar to the *a* axis of phase II, as illustrated in Fig. 6(b) by dotted lines. Therefore, the phase transformation from I ($Pa3$) to IV (*Pbcn*) can be understood in terms of counterrotations of CO_2 molecules (depicted by short arrows) to an intermediate state similar to phase II, followed by translations of half of the carbon atoms by half unit cell distance in a similar way to the phase-II–to–IV transition shown in Fig. 6(a).

Phase V ($P2_12_12_1$) is a 3D network structure with four coordinated carbon atoms and two coordinated oxygen atoms, while phase IV (*Pbcn*) can be considered as a 2D buckled layer structure. Six carbon dioxide molecules make a 12-member ring in phase V, whereas four molecules form an 8-member ring in phase IV. Then the structural difference between phases IV and V can be readily illustrated as shown in Fig. 6(c), by counteracting rotations of oxygen atoms (as depicted in arrows) and bridging oxygen atoms (depicted in circles) between two adjacent layers of the *ac* planes. However, because of a relatively large volume difference between phases IV and V (nearly 15%–20%), the IV-to-V phase transition will also involve diffusive motions of carbon and oxygen atoms.

The transitions between the $P4_12_12$ structure of phase IV and other phases are considered in similar ways. However, if the transformation from phase II is displacive, the O-C-O bending in phase IV doubles the *c* axis of phase II ($P4_2/mnm$ or *Pnnm*) by lowering the $4_2/m$ axis to a 4_1 axis and removing the *n* glide to a 2_1 screw. Similarly, the transition from phase I to IV ($P4_12_12$) is also expected to be displacive, involving rotations of oxygen atoms as shown in Fig. 6(b), followed by a doubling of the *c* axis due to the slight bending of the molecules.

We also note that all of the space groups are in subgroup and supergroup relationships as shown in Fig. 7. *Cmca* of phase III and $P4_2/mnm$ of phase II are subgroup of $Pa3$ of phase I. *Pbcn* of phase IV is a subgroup of *Cmca* of phase III and a supergroup of $P2_12_12_1$ of phase V through $P2_12_12$. Here $P2_12_12_1$ of phase V is also a subgroup of $P4_12_12$ of phase IV. However, the phase transitions between the *Pbcn* and other phases II ($P4_2/mnm$ or *Pnnm*), I ($Pa3$), or V ($P2_12_12_1$) are discontinuous and reconstructive. The transitions between the $P4_12_12$ to other phases are continuous and displacive. While the x-ray data do not distinguish between the $P4_12_12$ and *Pbcn*, the transition dynamics seems to favor the *Pbcn* structure for phase IV. That is, these and previous experiments[12,15,16] show that (1) the II-IV phase transition is very sluggish over a relatively large temperature range of between 30 and 50 K. (2) Phase IV can be quenched to ambient temperature without a back transformation to phase II. (3) Large grains of nearly optically isotropic phase IV are quite distinctive from highly polycrystalline phase II. (4) Significant volume changes are associated with the phase transitions among IV, II, and V (see Fig. 3). These experimental observations clearly imply that the transitions from phase IV to phases II and V are diffusive and thereby support the *Pbcn* structure for phase IV. Our recent observation of a similar *Pbcn* structure in N_2O-IV, an isoelectronic analog of CO_2-IV, further supports this conclusion.[30] Finally, single-crystal x-ray diffraction and infrared spectroscopy may provide further constraints for the structure of phase IV, although both growing a single crystal of phase IV and observing infrared bands near strong diamond absorptions are formidable experimental challenges.

SUMMARY

In this paper, we presented two plausible crystal structures for phase IV: the $P4_12_12$ and *Pbcn* structure that we prefer. We also discussed the transition pathways between CO_2-IV and its neighboring phases I, II, and V.

The crystal structure of CO_2-IV clearly represents an intermediate, as evident from its highly elongated intramolecu-

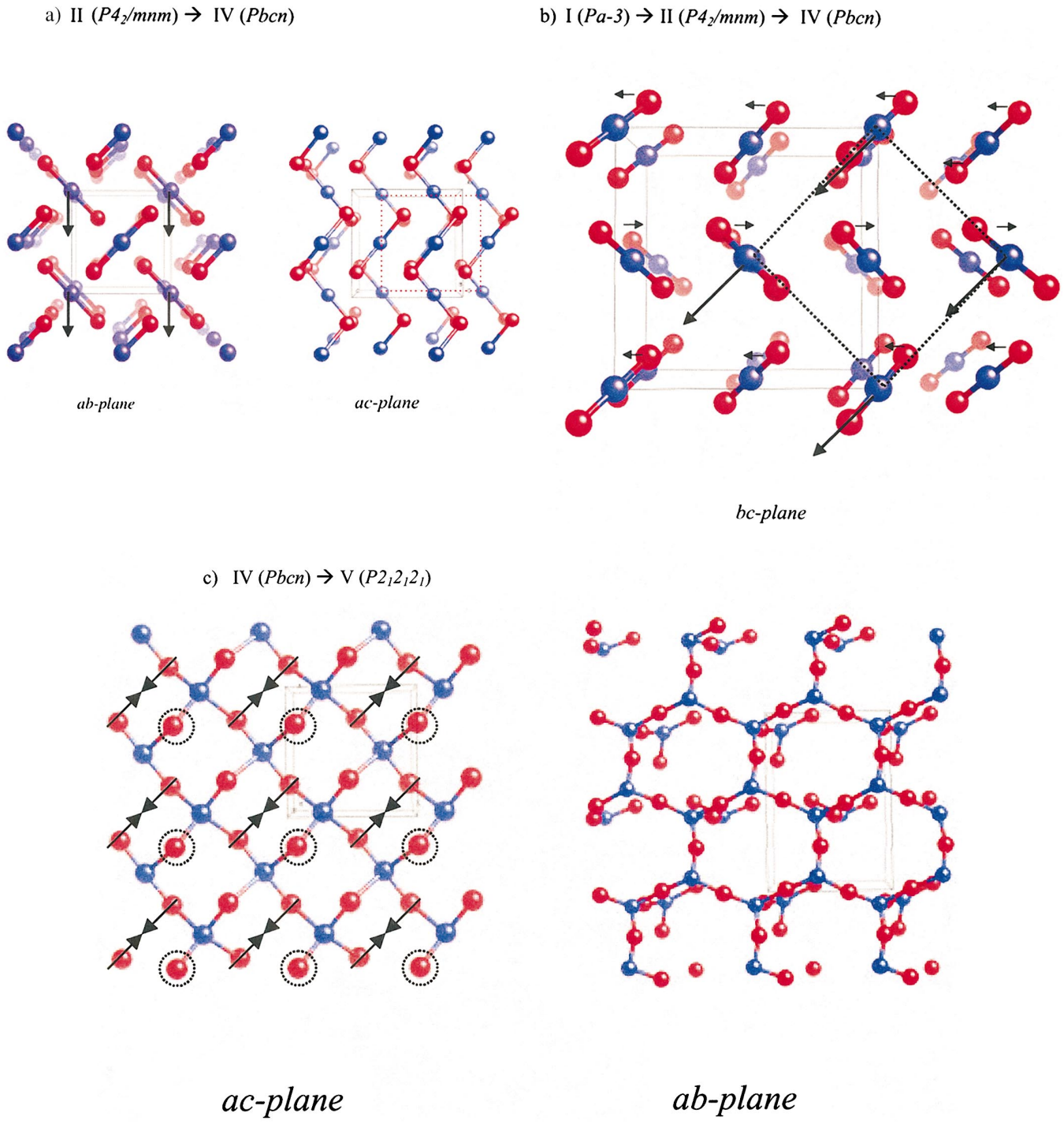

FIG. 6. (Color) Schematics to illustrate the transition dynamics between phase IV (*Pbcn*) and phase II (a), phase I (b), and phase V (c). Note that the transitions between the *Pbcn* and other phases are reconstructive with relatively large volume changes of 3 to 15%.

lar C-O bond length (~1.45 Å) and its collapsed intermolecular C···O distance (~2.0 Å). The bent molecular configuration in this phase clearly assists in lowering the activation barrier associated with the transition to phase V. Therefore, phase IV can be considered as a precursor to phase V. Carbon atoms in phase IV are coordinated with from four (up to first nearest neighbors) to six (up to second nearest neighbors) oxygen atoms, which results in the specific volume between phases II and III.

Despite the huge difference among their electronic structures, the crystal structures of CO_2 phases exhibit a great degree of similarity with those of many SiO_2 polymorphs. The examples include stishovite-like CO_2-II ($P4_2/mnm$), β-cristobalite-like ($P4_12_12$) or post-stishovite-like (*Pbcn*) CO_2-IV, tridymite-like CO_2-V ($P2_12_12_1$), and even α-cristobalite-like CO_2-I ($Pa3$) polymorphs. While the structures of CO_2 phases are isostructural (or close) to those of SiO_2 polymorphs, the nature of chemical bonding is

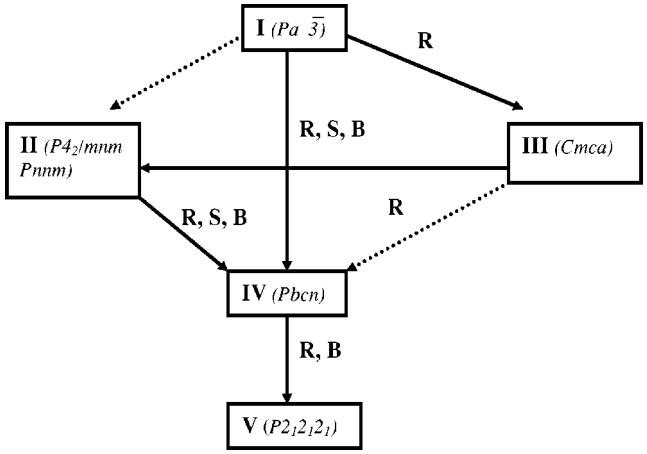

FIG. 7. Schematic to illustrate the sub- and super-group relationships of CO_2 phases. R, B and S respectively represent Rotation, Bending and Shift of atomic positions. Solid arrows illustrate experimentally observed phase transitions, whereas broken arrows the subgroup relationship of phases where no direct transitions were observed.

clearly different between CO_2 and SiO_2 polymorphs. With increasing pressure and temperature, the intermolecular bonding in CO_2 phases, for example, increases from nearly nonbonding in phase I to approximately a half-bonding in phases II and IV and to a full covalent bonding in phase V.

In short, the phase diagram of CO_2 coupled with detailed structural information provides insight into the molecular-to-nonmolecular transition. The present results indicate that pressure-induced electron delocalization in carbon dioxide occurs continuously via intermediate states like phases IV and II, rather than more abruptly within a single-step phase transition from a localized molecular phase to an itinerant extended phase. Such a continuous transformation of CO_2 is in a way analogous to SN-II type of polymerization, as opposite to SN-I type. According to this scheme, the final structure of the covalent solid is not uniquely determined by lowest-energy considerations, but may be strongly influenced by the existence of kinetic barriers between intermediate structures. Importantly, this result explains the observed overlaps in the stability domains of high-pressure phases (II, III, IV, V, and VI) and may be the reason why covalent CO_2 crystallizes in the tridymite structure rather than in the cristobalite structure, which was reported as the lowest-energy configuration for CO_4-based solids.[31]

ACKNOWLEDGMENTS

The x-ray work has been done at the ESRF and SSRL. We thank K. Visbeck at LLNL for assisting with the experiments. Numerous discussions with S. Bonev, G. Galli, and F. Gygi at LLNL have been very useful for the study. This work has been supported by the LDRD and PDRP programs at Lawrence Livermore National Laboratory, University of California, under the auspices of the U.S. Department of Energy under Contract No. W-7405-ENG-48 and DOE Cooperative Agreement No. DE-FC08-01NV14049 with the University of Nevada, Las Vegas.

[1] R. Reichlin, K. E. Brister, A. K. McMahan, M. Ross, S. Martin, Y. K. Vohra, and A. L. Ruoff, Phys. Rev. Lett. **62**, 669 (1989).
[2] K. A. Goettel, J. H. Eggert, I. F. Silvera, and W. C. Moss, Phys. Rev. Lett. **62**, 665 (1989).
[3] S. T. Weir, A. C. Mitchell, and W. J. Nellis, Phys. Rev. Lett. **76**, 1860 (1996).
[4] P. Loubeyre, P. Occellu, and R. LeToullec, Nature (London) **416**, 613 (2002).
[5] V. Iota, C. S. Yoo, and H. Cynn, Science **283**, 1510 (1998).
[6] C. S. Yoo, H. Cynn, F. Gygi, G. Galli, V. Iota, M. F. Nicol, S. Carlson, D. Hausermann, and C. Mailhiot, Phys. Rev. Lett. **83**, 5527 (1999).
[7] A. F. Goncharov, E. Gregoryanz, H. K. Mao, Z. Liu, and R. J. Hemley, Phys. Rev. Lett. **85**, 1262 (2000).
[8] M. L. Erements, R. J. Russell, H. K. Mao, and E. Gregoryanz, Nature (London) **411**, 170 (2001).
[9] C. Mailhiot, L. H. Yang, and A. K. McMahan, Phys. Rev. B **46**, 14 419 (1992).
[10] S. Serra, C. Cavazzoni, G. L. Chiarotti, S. Scandolo, and E. Tossatti, Science **284**, 788 (1999).
[11] B. Holm, R. Ahuja, A. Belomoshko, and B. Johansson, Phys. Rev. Lett. **85**, 1258 (2000).
[12] V. Iota and C. S. Yoo, Phys. Rev. Lett. **86**, 5922 (2001).
[13] A. Simon and K. Peters, Acta Crystallogr., Sect. B: Struct. Crystallogr. Cryst. Chem. **35**, 2750 (1980).
[14] K. Aoki, H. Yamawaki, M. Sajashita, T. Gotch, and K. Takemura, Science **263**, 356 (1994).
[15] C. S. Yoo, H. Kohlmann, H. Cynn, M. F. Nicol, V. Iota, and T. LeBihan, Phys. Rev. B **65**, 104103 (2002).
[16] C. S. Yoo, V. Iota, and H. Cynn, Phys. Rev. Lett. **86**, 444 (2001).
[17] O. Tschauner, H.-K. Mao, and R. J. Hemley, Phys. Rev. Lett. **87**, 075701 (2001).
[18] J. Yen and M. Nicol, J. Appl. Phys. **72**, 5535 (1992).
[19] A. P. Hemmersley (unpublished).
[20] A. C. Larson and R. B. von Dreele (unpublished).
[21] $R_{wp}=\mathrm{sqrt}\{[w(y_o-y_c)^2]/w(y_o)\}$, $R_p=ly_o-y_cl^2/y_o$, zero shift. The value of texture index in *sp*-preferred orientation with spherical harmonics means the degree of texture: 1 means no texture, 3 is strong texture, and higher than 3 means it may be overfitted [see R. B. Von Dreele, J. Appl. Crystallogr. **30**, 517 (1997)].
[22] R. W. G. Wyckoff, *Crystal Structure*, 2nd ed. (Wiley, New York, 1963), Vol. I, p. 312.
[23] J. Haines, J. M. Leger, and O. Schulte, J. Phys.: Condens. Matter **8**, 1631 (1996).
[24] J. S. Olsen, L. Gerward, and J. Z. Jiang, J. Phys. Chem. Solids **60**, 229 (1999).
[25] L. Liu, Phys. Earth Planet. Inter. **9**, 338 (1974).

[26] K. Suito, N. Kawai, and Y. Masuda, Mater. Res. Bull. **10**, 677 (1975).
[27] S. Endo, T. Nitawaki, Y. Akahama, T. Kikegawa, and O. Shimomura, High Press. Res. **4**, 408 (1990).
[28] J. Haines and J. M. Léger, Phys. Rev. B **55**, 11 144 (1997).
[29] A. H. Jay, Miner. Mag. **27**, 54 (1944).
[30] V. Iota, *et al.* (unpublished).
[31] J. Dong, J. K. Tomfohr, and O. F. Sankey, Phys. Rev. B **61**, 5967 (2000).